Journal of Solid State Chemistry 184 (2011) 1079–1084

Contents lists available at ScienceDirect

Journal of Solid State Chemistry

journal homepage: www.elsevier.com/locate/jssc

The pressure induced B1–B2 phase transition of alkaline halides and alkaline earth chalcogenides. A first principles investigation

Oliver Potzel, Gerhard Taubmann *

Institute of Theoretical Chemistry, D-89069 Ulm, Germany

ARTICLE INFO

Article history:
Received 18 November 2010
Received in revised form
8 March 2011
Accepted 13 March 2011
Available online 21 March 2011

Keywords:
Phase transition
DFT
Enthalpy of activation
Root of matrix

ABSTRACT

In this work, we considered the pressure induced B1–B2 phase transition of AB compounds. The DFT calculations were carried out for 11 alkaline halides, 11 alkaline earth chalcogenides and the lanthanide pnictide CeP. For both the B1 and the B2 structures of each compound, the energy was calculated as a function of the cell volume. The transition pressure, the bulk moduli and their pressure derivatives were obtained from the corresponding equations of state. The transition path of the Buerger mechanism was described using roots of the transition matrix. We correlated the computed enthalpies of activation to some structure defining properties of the compounds. A fair correlation to Pearsons hardness of the ions was observed.

1. Introduction

A pressure induced phase transition from the sixfold coordinated rock salt structure (B1, $Fm\bar{3}m$,#225) [1,2] to the eightfold coordinated CsCl structure (B2, $Pm\bar{3}m$,#221) can be observed for most alkaline halides and alkaline earth chalcogenides. Experimentally, transition pressures ranging from 0.5 GPa (RbBr) up to about 60 GPa (CaO) have been reported [3–19]. Many theoretical investigations concerning the transition pressures have been published [20–26], whereas only few papers considered the activation enthalpy [29,30]. A simple transition path between the B1 and the B2 structures can be described within the common subgroup $R\bar{3}m$ (# 166). This path is known as Buerger mechanism [31]. All transitions considered in this work occur along this path.

The computational effort of searching the optimum transition state can be reduced by modelling the path between B1 and B2 through roots of the transition matrix. It has been shown recently [32] for the examples of NaCl and CaO that this highly efficient method (MRAM) can be applied successfully to calculate enthalpies of activation within the Buerger mechanism.

This work shows a summary of calculated transition pressures and activation enthalpies for NaF, NaCl, all potassium and rubidium halides, CsF, all calcium and strontium chalcogenides, BaS, BaSe, BaTe and CeP. The alkaline halides and alkaline earth chalcogenides missing in this list do not undergo the pressure induced B1–B2 transition. The enthalpies of activation were correlated to the charge of the ions, to the cell volume and to Pearson's hardness [34].

The quantum chemical calculations in this work were carried out using the open source DFT code ABINIT [35] in which periodic boundary conditions, plane waves and pseudopotentials are used.

2. Transition pressures

We focus on the comparison of the numerous compounds given above. Therefore, the parameters of the calculations had to be chosen to give consistent results for all compounds instead of describing only a few of them with high precision. Preliminary computations were carried using both the local density approximation (LDA) and the general gradient approximation (GGA). The relative deviations of the cell volume at 0 K calculated with GGA from the experimental cell volume observed at standard conditions were always smaller than for the corresponding LDA results. The volumes from LDA were constantly about 10% too small as usually expected from overbinding, whereas for the GGA results deviations in both directions were found. Therefore, transition pressures for some compounds were calculated both from LDA and GGA in the way described below. In the case of RbBr, a negative transition pressure was obtained with GGA. Thus, LDA with the Hedin–Lundqvist functional [36] was used for all calculations reported in the following text.

Furthermore all input parameters concerning convergence such as *k*-points, Monkhorst Pack grid and cutoff energy were chosen high enough to obtain properly converged energies. The cutoff

* Corresponding author. Fax: +49 731 50 22819.
E-mail addresses: oliver.potzel@uni-ulm.de (O. Potzel), gerhard.taubmann@uni-ulm.de (G. Taubmann).

0022-4596/$ - see front matter © 2011 Elsevier Inc. All rights reserved.
doi:10.1016/j.jssc.2011.03.027

Table 1
Thermodynamical data calculated in this work.

Comp.	p_{trans} (GPa)		V_0 (B1) (Bohr^3)		B_0 (B1) (kbar)		B'_0 (B1)		V_0 (B2) (Bohr^3)		B_0 (B2) (kbar)		B'_0 (B2)		Ref.
	Calc.	Ref.	Calc.	Ref.	Calc.	Ref.	Calc.	Ref.	Calc.	Ref.	Calc.	Ref.	Calc.	Ref.	
NaF	23.3	23–26	154.2	166.4	630	435–465	4.6	4.4–5.3	138.8		677	494–1030	4.6	4	[4,5,21–23]
NaCl	27.1	27	275.7	302.7	319	235–320	4.7	4–5	259.0	277	356	344–373	4.5	4–4.3	[3,24]
KF	3.65	3.5–4	229.8	257.7	440	316–342	5.0	4.8–5.4	196.1		546	370	4.8	5.4	[5,7,8]
KCl	1.47	1.9	374.8	421.0	242	168–370	4.9	4.9–5.7	322.1	358–361	288	148–287	4.9	4.4–7	[5,9,10]
KBr	1.53	1.7–1.9	432.4	472.1	203	126–180	4.9	5.3–5.5	376.8		240		4.9		[8,9,25]
KI	1.78	1.8	531.3	577.2	160	105–141	4.9	5.4–5.6	472.9		188		4.9		[8,9,25]
RbF	2.74	2–3	273.5	294.4	391	277–315	5.0	5.1–5.7	234.5		477		5.0		[8,25]
RbCl	0.17	0.5	433.2	470.2	218	134–187	5.0	5.3–5.6	363.0		268		5.1		[8,9,25]
RbBr	0.16	0.5	494.7	535.6	184	108–160	5.1	5.5–5.6	418.4		226		5.1		[8,25]
RbI	0.18	0.3	600.3	646.4	147	86–131	5.1	5.6–5.8	515.0		180		5.1		[8,9,25]
CsF	3.64	2	329.4	366.2	341		5.2		289.9		422		5.2		[6,11]
CaO	59.5	60	175.2	187.7	1300	1110 ± 10	4.3	4.2 ± 0.2	155.1		1380	1300 ± 200	4.2	3.5 ± 0.5	[5,12]
CaS	39.3	37.1 ± 2.9	289.1	310.6	674	567–640	4.1	4.2–4.9	263.4	280	706	640	4.0	4.2	[5,13]
CaSe	39.7	30.2–39	326.3	349.3	575	510	4.1	4.2	300.6		602	510	4.0	4.2	[13]
CaTe	38.4	30–40	403.0	431.6	452	420 ± 30	4.0	4.3–5	375.4	375	473		4.1		[13,14]
SrO	30.9	36	216.6	231.8	1060	960 ± 24	4.5	4.4 ± 0.5	187.5	190	1160	1300	4.4	4.1	[5,15,21]
SrS	16.7	18	342.8	368.1	586	580	4.3		301.9		627		4.2		[16]
SrSe	16.2	14	382.7	408.7	503	452	4.3	4.5	341.1	361	538	465	4.2	4.5	[17]
SrTe	14.1	12 ± 1	465.3	498.2	397	395 ± 30	4.2		419.0	436	429		4.2		[14]
BaS	5.13	6–7.2	409.1	440.0	519	394–533	4.3	4.9–5.5	344.3	343–360	570	340–608	4.3	7.8	[5,18,27,28]
BaSe	5.05	5–6.1	451.3	484.0	449	382–460	4.5	4.4–5.3	384.3	380–425	495	419 ± 140	4.4		[18,27,28]
BaTe	4.16	4–5.5	539.0	580.5	363	288–357	4.4	4.5–5.4	464.1	426–526	405	275–394	4.3		[18,27,28]
CeP	21.1	19	315.8	337.8	798		5.1		273.5		968		4.6		[19]

energy was set to 200 Ha and its smearing to 0.1 Ha. We used a $2 \times 2 \times 2$ Monkhorst Pack grid for the k-points, which was shifted four times within each calculation. The break condition for the SCF calculations was 10^{-10} Ha.

We used fully relativistic norm conserving Hartwigsen, Goedecker, Hutter pseudopotentials [37] throughout the calculations. In order to get an equation of state for each compound in B1 and B2 structures, about 20 ground state energies were calculated for volumes reaching from $0.6V_0$ to $1.1V_0$, where V_0 denotes the cell volume at minimum energy. The resulting $E(V)$ data were fitted to the Birch–Murnaghan equation of state [38,39]

$$E_{BM}(V) = E_0 + \frac{9}{16}V_0B_0\left\{\left[\left(\frac{V_0}{V}\right)^{2/3}-1\right]^3 B_1 + \left[\left(\frac{V_0}{V}\right)^{2/3}-1\right]^2 \cdot \left[6-4\left(\frac{V_0}{V}\right)^{2/3}\right]\right\} \quad (1)$$

The $E(V)$ curves were described using Eq. (1) with the parameters obtained from a nonlinear least squares fit. In every point of the $E(V)$ curves the pressure p is given as

$$-p = \left(\frac{\partial A}{\partial V}\right)_T = \frac{dE}{dV} \quad (2)$$

The free energy is denoted by A, which equals E at $T=0$ K.

Subsequently the transition pressures p_{trans} were calculated from the slope of the common tangent to the $E(V)$ curves of both the B1 and the B2 structures. Table 1 shows a summary of the thereby calculated thermodynamic properties of all investigated compounds.

3. Enthalpies of activation

Pressure conditions which are necessary to induce structural phase transitions occur in various depths of the earth's mantle and can be realized with diamond anvil cells [40] in the laboratory. Transition pressures have been widely examined both experimentally and theoretically for many different compounds.

The transition mechanism in contrast, cannot be observed directly in experiments and therefore only few papers refer to the transition path [29,30]. As early as 1948 Buerger [31] suggested a first simple path from B1 to B2. This path is based on the increase of the rhombohedral angle from 60° in the primitive B1 cell to 90° in the B2 cell. Within this path, all intermediate structures belong to the space group $R\bar{3}m$ (# 166), which is a subgroup common to $Fm\bar{3}m$(#225) and $Pm\bar{3}m$(#221).

In the following, Wanatanabe et al. [41] reported a further possible transition path via the common subgroup $Pmmn$ (#59). Finally, Stokes and Hatch [42] mathematically investigated all possible mechanisms between B1 and B2 and reported for the example of NaCl the transition in the subgroup $P2_1/m$ (#11) with the lowest enthalpy of activation. However, according to molecular dynamics simulations [43] the Buerger mechanism is one of the most favourable.

In a previous paper [32] we showed that the path within the Buerger mechanism can be evaluated through roots of the transition matrix without the computational cost of a structure optimization procedure. This matrix root application method (MRAM) is based on the fact that both the starting structure B1 and the target structure B2 can be given by the matrices $\mathbf{B}_1$ and $\mathbf{B}_2$ of their primitive cell vectors. The phase transition can then be described by a transformation matrix $\mathbf{T}$ with $\mathbf{B}_1 = \mathbf{B}_2\mathbf{T}$. In our case, the matrices are

$$\mathbf{B}_1 = \mathbf{T} = \begin{pmatrix} 0 & \frac{1}{2} & \frac{1}{2} \\ \frac{1}{2} & 0 & \frac{1}{2} \\ \frac{1}{2} & \frac{1}{2} & 0 \end{pmatrix} \quad \text{and} \quad \mathbf{B}_2 = \begin{pmatrix} 1 & 0 & 0 \\ 0 & 1 & 0 \\ 0 & 0 & 1 \end{pmatrix} \quad (3)$$

The MRAM uses higher roots $\mathbf{R} = \mathbf{T}^{1/n}$ of the transformation matrix $\mathbf{T}$ in order to create an arbitrary number $(n-1)$ of intermediate structures between B1 and B2. The transition path can be reproduced sufficiently accurate using about 10 intermediate steps between the starting structure and the target structure. In most calculations reported in the literature, nine intermediate structures corresponding to 10 steps were used. In our calculations, we thus decided to use the tenth root ($n=10$).

The cell constants of the cubic B1 and B2 structures were obtained from the points of contact of the common tangent to the $E(V)$-curves of both structures and are denoted as a_{B1} and a_{B2}, respectively. This method guarantees that the enthalpies in both

contact points are identical. Table 1 lists the cell volumes of all compounds investigated in this work. The matrices $\mathbf{C}_n$ of the primitive vectors of the intermediate structures within the Buerger mechanism are then given by

$$\mathbf{C}_n = a_{\mathrm{B1}} c^n \mathbf{B}_2 \overline{\mathbf{R}}^{10-n} \quad (n = 1,2,\ldots,9), \quad c = \sqrt[10]{\frac{a_{\mathrm{B2}}}{a_{\mathrm{B1}}}}. \tag{4}$$

The initial B1 structure corresponds to $n=0$ and the final B2 structure is described by $n=10$.

Like numbers, matrices have several roots. Beyond this discrete multiplicity found for every root of any matrix, the roots of $\mathbf{T}$ do also depend on a continuous parameter, because one of the eigenvalues of $\mathbf{T}$ is doubly degenerate [32,44]. This allows the root to be chosen as

$$\overline{\mathbf{R}} = \begin{pmatrix} a & b & c \\ c & a & b \\ b & c & a \end{pmatrix} \quad \text{where} \quad \begin{aligned} a &= 0.924911 \\ b &= 0.204008 \\ c &= -0.128919 \end{aligned} \tag{5}$$

Details of the derivation of $\overline{\mathbf{R}}$ can be found in [32]. The symmetric form of $\overline{\mathbf{R}}$ has to be chosen because the primitive vectors are equal in length within the common subgroup $R\bar{3}m$. With the numerical values of a–c listed in (5), the sequence of the $\mathbf{C}_n$ in Eq. (4) describes a smooth transition between the B1 and the B2 structures. According to the properties of spacegroup $R\bar{3}m$, the positions of the ions were constrained throughout the transition to $(0,0,0)$ for the anion and $(1/2,1/2,1/2)$ for the cation. The groundstate energies E_n and the volumes V_n of all structures given by $\mathbf{C}_n$ (n=0–10) were used to calculate the corresponding enthalpies H_n from

$$H_n = E_n - p_{\mathrm{trans}} V_n \quad \text{with } p_{\mathrm{trans}} = -\frac{E_{10}-E_0}{V_{10}-V_0} \tag{6}$$

As the common tangent method was used, the enthalpies of the starting structure and of the target structure are equal $H_0=H_{10}$.

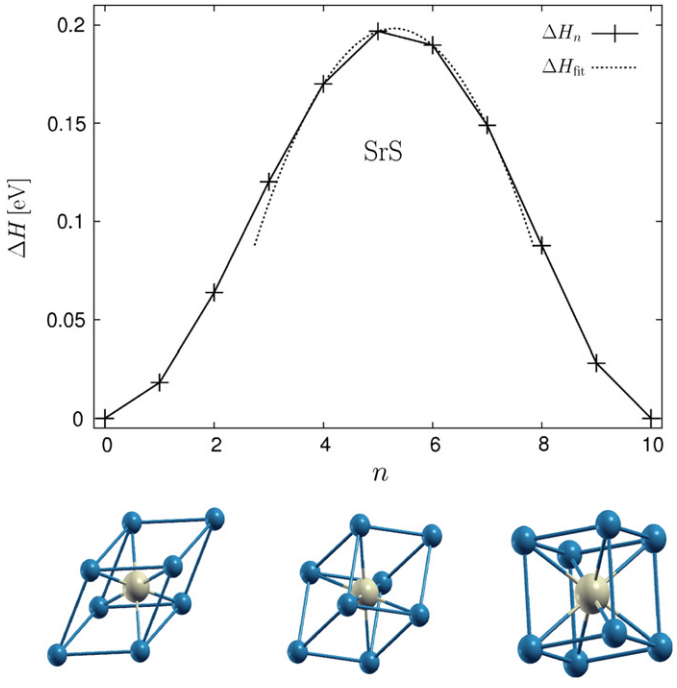

Fig. 1. Shown is the ΔH_n curve for SrS together with the interpolating parabola ΔH_{fit} through the three points (n=4–6) of maximum enthalpy. The enthalpy of activation obtained from this curve is $\Delta H^{\neq} = 0.198$ eV. The primitive cells of the initial and the final states together with the structure of the transition state are shown below the curve near the corresponding value of n.

The enthalpy of activation $\Delta H^{\neq}$ is given by the maximum of the ΔH_n curve, where $\Delta H_n = H_n - H_0$. A sufficiently accurate value of $\Delta H^{\neq}$ can be obtained by parabolic interpolation between the three points of highest ΔH_n. A ΔH_n curve together with the interpolating parabola is shown in Fig. 1 for the example of SrS. It is worth noting that the structures with highest enthalpies were always found somewhere between $\mathbf{C}_4$ and $\mathbf{C}_6$. The maxima were found at $\mathbf{C}_6$ for the alkaline halides, at $\mathbf{C}_5$ for the alkaline earth chalcogenides and at $\mathbf{C}_4$ in the case of CeP. This spread range shows that a root like $\overline{\mathbf{R}}$ in the order of a tenth root is necessary in order to locate the relevant intermediate structure. A square root revealing only a single interjacent structure would certainly not be enough.

4. Results

In this work the transition pressures and enthalpies of activation were calculated for the pressure induced B1–B2 phase transition within the Buerger mechanism for 11 alkaline halides, 11 alkaline earth chalcogenides and the lanthanide pnictide CeP. All the alkaline halides and alkaline earth chalcogenide not included in this work either do not undergo a pressure induced B1–B2 phase transition or reliable reference data are lacking (MgO) [33].

All transition pressures listed in Table 1 differ only slightly both from the experimental values and from other theoretical data from the literature. Thus, based on the calculated transition pressures, consistent data for the activation enthalpies can be obtained. It is worth noting that most of the bulk moduli calculated for the B1 structures are at the upper limit or above the reference values, whereas the corresponding B_0' values are situated near or below the lower limit of the values given in the literature.

The $\Delta H^{\neq}$ values determined in this work are listed in Table 2. No experimental values could be found in the literature. The calculated values vary up to a factor of six between a minimum of 0.04 eV for CsF and a maximum of 0.23 eV for CaO. Thus, an attempt was made to correlate $\Delta H^{\neq}$ to some properties of the compounds.

As anions and cations move relative to each other during the transition, a dependence proportional to Z^2 according to Coulomb's law can be expected, Z being the charge of the ions.

It can be seen from Table 2 that a crude approximation of $\Delta H^{\neq}$ is given by

$$\Delta H^{\neq} \approx 0.05\ \mathrm{eV} \cdot Z^2 \tag{7}$$

Table 2
Enthalpies of activation calculated for the alkaline halides (MX) and alkaline earth chalcogenides $\tilde{M}\tilde{X}$.

M	X			
	F	Cl	Br	I
Na	0.0791	0.0685		
K	0.0675	0.0612	0.0553	0.0483
Rb	0.0590	0.0641	0.0590	0.0517
Cs	0.0397			
$\tilde{M}$	$\tilde{X}$			
	O	S	Se	Te
Ca	0.2337	0.2259	0.2312	0.2315
Sr	0.2038	0.1968	0.1905	0.1801
Ba		0.1792	0.1745	0.1635

The $\Delta H^{\neq}$ values are given in eV.

The transition within the Buerger mechanism consists of a compression along the space diagonal in the unit cell. Therefore, the transition should be energetically preferred if the ions on the octahedral sites can easily follow this deformation. This occurs if the octahedral holes are large compared to the volume of the smaller ions. The enthalpies of activation should thus rise with increasing radius ratio $q = r_{cat}/r_{an}$ between cations and anions [45]. It is worth noting that the cation is larger than the anion in KF, RbF and CsF and $q > 1$ is observed. Thus, the radius ratio $\tilde{q} = r_< / r_>$ between the smaller ion and the larger ion is used for the alkaline halides. The $\Delta H^{\neq}$ values are shown as a function of $\tilde{q}$ or q for the alkaline halides and the alkaline earth chalcogenides in Figs. 2 and 3, respectively.

It can be seen from these figures that the dependence of $\Delta H^{\neq}$ on $\tilde{q}$ usually follows the trend we expect. Deviations were found only for compounds with exceptional radius ratios such as CaSe and CaTe (very small q) or for RbF and CsF (q considerably larger than one). Needless to say that no trend can be observed for the only caesium compound CsF, which was listed with the exceptions only because of its very large value of $q = 1.26$. Within the row of the alkali fluorides with the very small and very hard anion F^-, the enthalpies of activation decrease with the size of the cation as can be seen best from Table 2. The deviations observed for the heavy calcium chalcogenides can be explained by the polarizing effect of the very small Ca^{2+} cation on the large soft anions which gives rise to covalent contributions to the chemical bond.

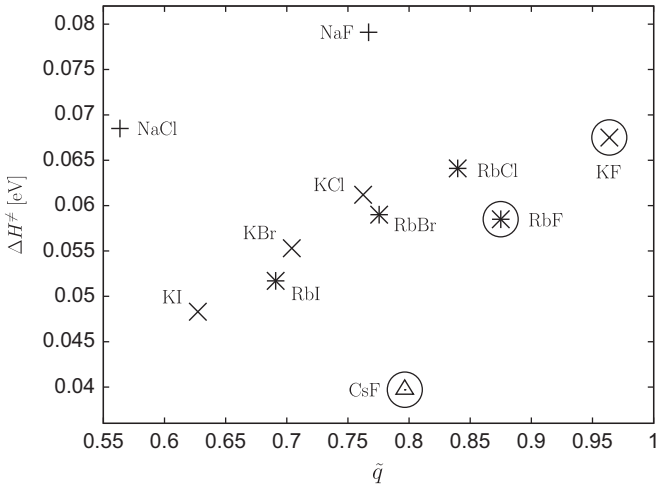

Fig. 2. The enthalpies of activation $\Delta H^{\neq}$ of the alkaline halides are shown as a function of the radius ratio $\tilde{q} = r_< / r_>$ of the small ion (radius $r_<$) and of the large ion (radius $r_>$). Compounds with the same kind of cation are drawn with identical symbols. The data points marked with circles represent compounds in which the cation is larger than the anion. In this case, we choose $\tilde{q} = 1/q$. As explained in the text, the $\Delta H^{\neq}$ values of the halides of a particular alkaline metal increase with $\tilde{q}$. The only exception from this trend was found for RbF.

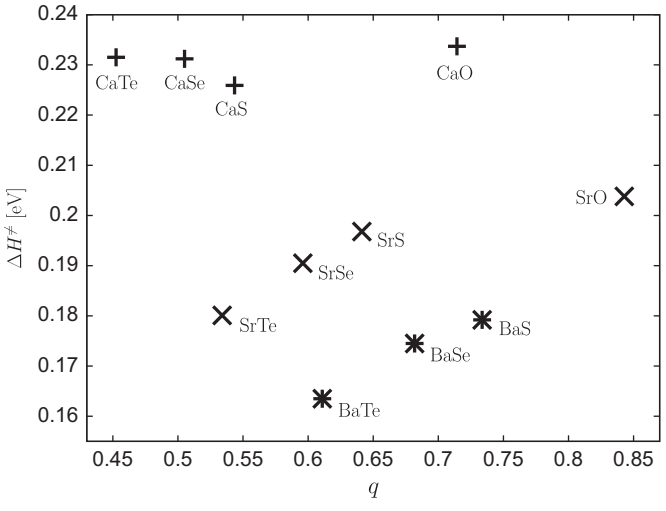

Fig. 3. Shown are the enthalpies of activation $\Delta H^{\neq}$ of the alkaline earth chalcogenides as a function of the radius ratio $q = r_{cat}/r_{an}$. Each kind of cation is indicated by a different symbol. The $\Delta H^{\neq}$ values of all chalcogenides of strontium and barium increase with q. The two calcium compounds with the large anions (CaSe and CaTe) which do not follow a similar trend have very low values of q. A very small cation has a strong polarizing effect on the large anions and covalent contributions to the chemical bond cannot be neglected any longer.

For compounds with exceptional radius ratios such as CaSe and CaTe (very small q) or for RbF and CsF (q considerably larger than one). Needless to say that no trend can be observed for the only caesium compound CsF, which was listed with the exceptions only because of its very large value of $q = 1.26$. Within the row of the alkali fluorides with the very small and very hard anion F^-, the enthalpies of activation decrease with the size of the cation as can be seen best from Table 2. The deviations observed for the heavy calcium chalcogenides can be explained by the polarizing effect of the very small Ca^{2+} cation on the large soft anions which gives rise to covalent contributions to the chemical bond.

As Coulomb forces abate with increasing distances between the ions, we correlated the enthalpies of activation $\Delta H^{\neq}$ to the volume V_{tr}^{B1} of the unit cell of the B1 structure at p_{trans}. Regression lines through the data of the alkaline halides and through the values of the chalcogenides of strontium and barium were calculated. The $\Delta H^{\neq}$ values of the calcium chalcogenides exhibit nearly no dependence on V_{tr}^{B1}, and were therefore not included in the latter least squares fit.

The radius ratios r_{cat}/r_{an} between cations and anions of the compounds considered in this work are considerably smaller for divalent ions than for univalent ions. Therefore, a strong dependence of $\Delta H^{\neq}$ on the anion can be expected for the alkaline earth chalcogenides. Smooth interpolating curves between the $\Delta H^{\neq}$ values of the oxides, sulphides, selenides and tellurides of the alkaline earth chalcogenides can be drawn in order to show the monotonic dependence. The results are shown in Fig. 4.

According to Pearson [34] atoms, ions, molecules and radicals can be characterized by their absolute hardness η and their electronic chemical potential μ. The abstract definitions of η and μ are

$$\mu = \left(\frac{\partial E}{\partial N}\right)_v \quad \eta = \frac{1}{2}\left(\frac{\partial \mu}{\partial N}\right)_v \tag{8}$$

with the number of electrons N and v being the external potential in the framework of DFT. For electrically neutral species X, η can be expressed approximately by

$$\eta_X \approx \tfrac{1}{2}(I_X - A_X) \tag{9}$$

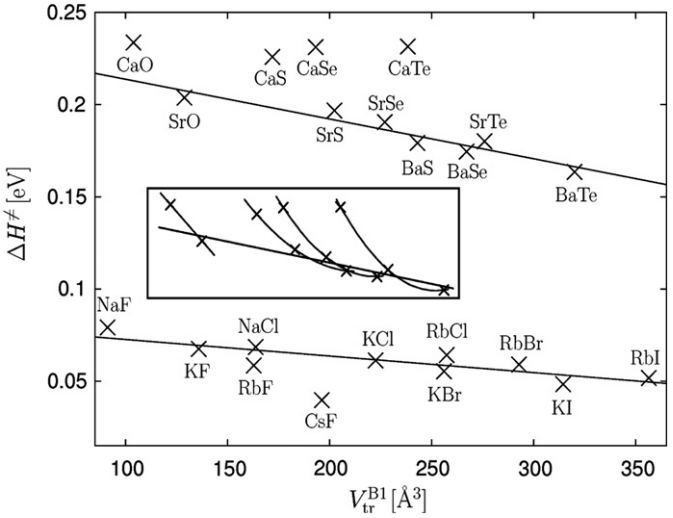

Fig. 4. Shown are the enthalpies of activation $\Delta H^{\neq}$ as a function of V_{tr}^{B1} for all alkaline halides and alkaline earth chalcogenides considered in this work together with the two regression lines mentioned in the text. The small box inserted in the centre shows the region of the alkaline earth chalcogenides, together with interpolating curves between the values of all oxides, sulphides, selenides and tellurides (from left to right).

where I_X and A_X denote the ionization energy and the electron affinity of X, respectively. As the electron affinities of anions are not known, Eq. (9) cannot be used in this case. Instead, the hardness of the neutral species is used as an approximate value [34,46]. The numerical values of η used are listed in Table 3 [46].

During the phase transition, the atoms are in very close contact to each other. Thus, they are at least slightly deformed which is easier in the case of soft ions than for hard ones. Therefore, we assumed a linear relation between $\Delta H^{\neq}$ and $x_{\mathrm{red}} = Z^2(\eta_+ + \eta_-)$. Fig. 5 shows $\Delta H^{\neq}$ as a function of x_{red} together with the regression line. It can be seen that the $\Delta H^{\neq}$ values of both the MX and $\tilde{M}\tilde{X}$ compounds are approximately given by the following equation:

$$\Delta H^{\neq} = k \cdot x_{\mathrm{red}} + c$$

$$k = 0.00220(4), \quad c = 0.017(3)\ \mathrm{eV} \mathrel{\hat{=}} 200\ \mathrm{K} \tag{10}$$

of the regression line. The value of c which is positive and close to zero indicates reasonable physical behaviour. Even nonionic compounds such as the noble gas neon [47] can undergo a temperature induced phase transition at very low temperatures. We therefore expect a positive value of the constant c, presuming $\eta > 0$ [34].

The value of CeP was not included in the fit used to obtain Eq. (10). It is the only compound considered in this work which is formally trivalent. In reality, the true charge of the ions in CeP is certainly less than three. Hypothetical charges of $Z = \pm 2.7$ for Ce and P, respectively, lead to a corrected data point lying exactly on the regression line.

Table 3
Absolute hardnesses η according to Adams [46].

Cation	η_+ (eV)	Anion	η_- (eV)
Na^+	21.07	F^-	7.01
K^+	13.65	Cl^-	4.68
Rb^+	11.56	Br^-	4.23
Cs^+	9.63	I^-	3.70
Ca^{2+}	19.52	O^{2-}	6.08
Sr^{2+}	15.93	S^{2-}	4.14
Ba^{2+}	13.65	Se^{2-}	3.87
		Te^{2-}	3.52
Ce^{3+}	8.28	P^{3-}	4.87

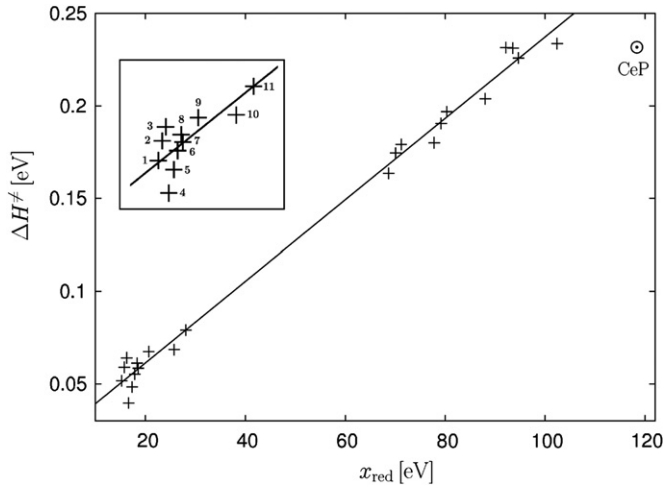

Fig. 5. Shown are the enthalpies of activation $\Delta H^{\neq}$ of all compounds considered in this work as a function of $x_{\mathrm{red}} = Z^2(\eta_+ + \eta_-)$, Z being the charge of the cations and η_+ and η_- being Pearson's hardnesses as listed in Table 3. The value of the lanthanide pnictide CeP is shown in a small circle. The region of the values for the alkaline halides is shown enlarged in the small box. The labels correspond to (1: RbI), (2: RbBr), (3: RbCl), (4: CsF), (5: KI), (6: KBr), (7: KCl), (8: RbF), (9: KF), (10: NaCl) and (11, NaF).

5. Conclusion

The MRAM method was applied successfully to the calculation of enthalpies of activation of various binary compounds. We considered the pressure induced phase transitions of alkaline halides, alkaline earth chalcogenides and CeP for the Buerger mechanism. The low computational costs of our method allowed these investigations on the large number of compounds.

The computed values of $\Delta H^{\neq}$ vary between nearly zero (0.04 eV for CsF) and 0.23 eV (for CaO). The $\Delta H^{\neq}$ correlated to Z^2 and to $x_{\mathrm{red}} = Z^2(\eta_+ + \eta_-)$ with fair success.

An extension of this work to other mechanisms [41,42] is currently under way.

Acknowledgments

The authors wish to thank Christian Carbogno and Jürgen Vogt for helpful discussions and Axel Groß for his aid in this work.

References

[1] ⟨http://www.cryst.ehu.es/⟩, last access: March 17, 2011.
[2] M.I. Aroyo, J.M. Perez-Mato, C. Capillas, E. Kroumova, S. Ivantchev, G. Madariaga, A. Kirov, H. Wondratschek, Z. Kristallogr. 221 (2006) 15–27.
[3] X. Li, R. Jeanloz, Phys. Rev. B 36 (1987) 474–479.
[4] Y. Sato-Sorensen, J. Geophys. Res. 88 (1983) 3543–3548.
[5] E. Knittel, Mineral Physics and Crystallography: A Handbook of Physical Constants, American Geophysical Union, Washington, DC, 1995.
[6] C.W.F.T. Pistorius, Prog. Solid State Chem. 11 (1976) 1–151.
[7] T. Yagi, J. Phys. Chem. Solids 39 (1978) 563–571.
[8] U. Köhler, P.G. Johannsen, W.B. Holzapfel, J. Phys. Condens. Matter 9 (1997) 5581–5592.
[9] G. Slack, R. Ross, J. Phys. C: Solid State Phys. 18 (1985) 3957–3980.
[10] D. Walker, L.M.D. Cranswick, P.K. Verma, S.M. Clark, S. Buhre, Am. Mineral. 87 (2002) 805–812.
[11] G.J. Piermarini, J. Res. Natl. Inst. Stand. Technol. 106 (2001) 889–920.
[12] P. Richet, H.K. Mao, P.M. Bell, J. Geophys. Res. 93 (1989) 15279–15288.
[13] H. Luo, R.G. Green, K. Ghandehari, T. Li, A.L. Ruoff, Phys. Rev. B 50 (1994) 16232–16237.
[14] H.G. Zimmer, H. Winzen, K. Syassen, Phys. Rev. B 32 (1985) 4066–4070.
[15] Y. Sato, R. Jeanloz, J. Geophys. Res. 86 (1981) 11773–11778.
[16] K. Syassen, Phys. Status Solidi A 91 (1985) 11–15.
[17] H. Luo, R.G. Green, A.L. Ruoff, Phys. Rev. B 49 (1994) 15341–15343.
[18] G. Kalpana, B. Palanivel, M. Rajagopalan, Phys. Rev. B 50 (1994) 12318–12325.
[19] I. Vedel, A.M. Redon, J. Rossat–Mignot, O. Vogt, J.M. Leger, J. Phys. C 20 (1987) 3439–3444.
[20] Z. Fang, I.V. Solovyev, H. Sawada, Phys. Rev. B 59 (1999) 762–774.
[21] R.L. Erikson, L.E. Eary, C.J. Hostetler, J. Chem. Phys. 99 (1993) 336–344.
[22] L.L. Boyer, Phys. Rev. B 23 (1981) 3673–3685.
[23] B. Rayo, S.P. Sanyal, Phys. Rev. B 42 (1990) 1810–1816.
[24] H. Zhang, M.S.T. Bukowinski, Phys. Rev. B 44 (1991) 2495–2503.
[25] K. Doll, H. Stoll, Phy. Rev. B 57 (1998) 4327–4331.
[26] J.C. Schön, Z. Anorg. Allg. Chem. 630 (2004) 2354–2366.
[27] B.S. Arya, M. Aynyas, S.P. Sanyal, Ind. J. Pure Appl. Phys. 46 (2008) 722–726.
[28] A. Bouhemadou, R. Khenata, F. Zegrar, M. Sahnoun, H. Baltache, A.H. Reshak, Comput. Mater. Sci. 38 (2006) 263–270.
[29] M. Catti, Phys. Rev. B 68 (2003) 100101.
[30] M. Catti, J. Phys. Condens. Matter 16 (2004) 3909–3921.
[31] J. Buerger, Phase Transformation in Solids, in: R. Smoluchowski (Ed.), Wiley, New York, 1951, pp. 183–211.
[32] O. Potzel, G. Taubmann, J. Phys. Condens. Matter 21 (2009) 245404.
[33] A. Hachemi, A. Saoudi, L. Louail, D. Maouche, A. Bouguerra, Phase Transitions 82 (2009) 87–97.
[34] R.G. Pearson, Inorg. Chem. 27 (1988) 734–740.
[35] X. Gonze, J.-M. Beuken, R. Caracas, F. Detraux, M. Fuchs, G.-M. Rignanese, L. Sindic, M. Verstraete, G. Zerah, F. Jollet, M. Torrent, A. Roy, M. Mikami, P. Ghosez, J.-Y. Raty, D.C. Allan, Comput. Mater. Sci. 25 (2002) 478–492.
[36] L. Hedin, B.I. Lundqvist, J. Phys. C Solid State Phys. 4 (1971) 2064–2083.
[37] C. Hartwigsen, S. Goedecker, J. Hutter, Phys. Rev. B 58 (1998) 3641–3662.
[38] F.D. Murnaghan, Proc. Natl. Acad. Sci. 30 (1944) 244–247.

[39] F. Birch, Phys. Rev. 71 (1947) 809–824.
[40] D.R. Allan, R. Miletich, R.J. Angel, Rev. Sci. Instrum. 67 (1995) 840–842.
[41] M. Wanatanabe, M. Tokonami, N. Morimoto, Acta Crystallogr. A 33 (1977) 294–298.
[42] H.T. Stokes, D.M. Hatch, Phys. Rev. B 65 (2002) 114114.
[43] S. Zhang, N.-X. Chen, Modelling Simul. Mater. Sci. Eng. 11 (2003) 331–338.
[44] F.R. Gantmacher, Matrix Theory, vol. 1, Chelsea, New York, 1960.
[45] R.D. Shannon, Acta Crystallogr. A 32 (1976) 751–767.
[46] S. Adams, Habilitation dissertation: Bindungsvalenzmodelle für Struktur–Leitfähigkeit–Beziehungen in Festkörperelektrolyten, Göttingen, 2000. 〈http://kristall.uni-mki.gwdg.de/〉, last access: March 17, 2011.
[47] E. Schuberth, M. Creuzburg, W. Müller–Lierheim, Phys. Status Solidi B 76 (1976) 301–306.